Ocean Engineering 243 (2022) 110165

Contents lists available at ScienceDirect

Ocean Engineering

journal homepage: www.elsevier.com/locate/oceaneng

A unified ship manoeuvring model with a nonlinear model predictive controller for path following in regular waves

R. Sandeepkumar [a], Suresh Rajendran [b,*], Ranjith Mohan [a], Antonio Pascoal [c]

[a] Department of Aerospace Engineering, Indian Institute of technology Madras, 600036 Chennai, India
[b] Department of Ocean Engineering, Indian Institute of technology Madras, 600036 Chennai, India
[c] Laboratory of Robotics and Engineering Systems (LARSyS), ISR/IST, University of Lisbon, 1649-004 Lisbon, Portugal

ARTICLE INFO

Keywords:
Unified seakeeping and manoeuvring model
KVLCC2
Model predictive control
Nonlinear MPC
PID
LOS
Path following
Regular waves

ABSTRACT

In this paper, a nonlinear model predictive controller for path following of a surface vessel in the presence of regular waves is studied. A model predictive controller is developed for a 3DoF unified manoeuvring model of the KVLCC2 crude oil tanker. The surge, sway and yaw motions of the ship are influenced by the second order wave drift forces and moments calculated based on a potential flow solver. Propeller thrust, rudder and hydrodynamic forces and moments are computed using empirical formulas available in the literature. For path following purposes, waypoints are assigned in head and beam wave conditions and a line of sight algorithm computes the reference heading angle. The rudder control is exerted by a nonlinear model predictive controller and the effectiveness of the controller is studied. The performance of the nonlinear model predictive controller is compared against that of a basic PID controller.

1. Introduction

Manoeuvring and seakeeping of ships are problems of different time scales that are independently studied to determine their behaviour. Traditionally, manoeuvring studies are conducted in calm water in places like harbours, where navigation space is limited and the effect of waves is negligible. On the other hand, in the open sea, the effects of wave forces are predominant and seakeeping becomes essential. However, with the recent regulations by the International Maritime Organisation (IMO) to regulate carbon emissions and improve the fuel efficiency of ships, manoeuvring in waves has attracted the attention of the international community. In this paper, a nonlinear model predictive control (NMPC) technique is applied to the unified seakeeping and manoeuvring model for the path following problem of a ship in regular waves. The advantage of a unified model is that it improves the accuracy of the system dynamics modelling through accurate estimation of the nonlinear wave loads.

1.1. Ship dynamics

The manoeuvrability of ships in calm water has been studied extensively using numerical simulation and experiments. Numerical simulations using mathematical models have been investigated in Son and Nomoto (1981), Yoshimura (2001), Xiang and Faltinsen (2011), Yasukawa and Yoshimura (2015), Sutulo and Soares (2019) and in Skjetne et al. (2004), Moreira and Soares (2011), Perera et al. (2012), Kim et al. (2019) experimental studies have been performed. The ship dynamics model is governed by nonlinear coupled differential equations (state-space formulation). A popular and widely used model for a ship heading control design is the first order Nomoto model (Nomoto and Taguchi, 1957) due to its simplicity and the potential to yield a simple controller with course keeping capabilities for small rudder angles. 3DoF Abkowitz models are generally considered adequate for ship manoeuvring studies (Lewis et al., 1988). The extension from 3DoF to 4DoF models (Son and Nomoto, 1981; Oltmann, 1993) becomes important when roll motion is significant, particularly for ships at higher speeds. Ship manoeuvring dynamics are complicated due to the nonlinear hydrodynamic effects. As a result, coupled nonlinear differential equations must be solved for numerical open-loop simulation studies.

1.2. Wave modelling

By including the wave forces and moments in the state-space model, the open-loop response of ships under known control inputs can be simulated and the response can be studied. The motion of ships in waves

* Corresponding author.
E-mail addresses: ae17s017@smail.iitm.ac.in (R. Sandeepkumar), sureshr@iitm.ac.in (S. Rajendran), ranjith.m@iitm.ac.in (R. Mohan), antonio@isr.ist.utl.pt (A. Pascoal).

https://doi.org/10.1016/j.oceaneng.2021.110165
Received 17 May 2021; Received in revised form 2 October 2021; Accepted 5 November 2021
Available online 1 December 2021

Nomenclature

$(*)_{\pm}$	upper/lower bounds
$\bar{x}$, $\bar{u}$	state and control input
$\bar{x}_r$, $\bar{u}_r$	Reference $\bar{x}$, $\bar{u}$
β	sideslip
χ	wave encounter angle
δ	rudder angle
Δ_h	look ahead distance
ϵ	ratio of wake fraction at propeller and rudder positions
η	ratio of propeller diameter to rudder span
γ	wave incidence angle
$\hat{x}$	state estimate
λ	wavelength of the wave
ω	frequency of the wave
ψ	heading angle
ρ	water density
A_R	profile area of movable part of mariner rudder
d	ship draft
D_P	propeller diameter
e	cross-track error
H	height of the wave
I_{zG}	moment of inertia
J_P	propeller advance ratio
J_z	added moment of inertia
K_T	propeller thrust open water characteristic
$K_{p,i,d}$	PID gains
L_{pp}	ship length
m	mass of the ship
$m_{x,y}$	added mass along x,y
N	Grid size
n_P	propeller RPS
P_k	kth waypoint
Q, R, S	weighting matrices
r	yaw rate
R_a	radius of acceptance
T	thrust
T_P	prediction horizon
t_P	thrust reduction factor
t_R	steering resistance deduction factor
T_s	sampling time
U	total speed
u, v	surge and sway velocities
W	Decision variable vector
w_P	wake coefficient at propeller position
x_G	x coordinate of centre of gravity
x_H	longitudinal coordinate of acting point of the additional lateral force
x'_P	longitudinal coordinate of propeller
AD	automatic differentiation
MIMO	multiple input multiple output
NMPC	nonlinear model predictive control
OCP	optimal control problem
QP	quadratic program
SISO	single input single output

is investigated in Bailey (1997), where a unified manoeuvring and seakeeping model is deployed and convolution type integral functions are used to represent hydrodynamic forces and moments. Nonlinear restoring and Froude–Krylov forces are calculated based on the estimation of the exact wetted surface area. However, such a body nonlinearity cannot completely capture the second order mean wave drift forces. The representation of radiation forces through a convolution integral facilitates accurate estimation of the linear radiation forces in irregular waves since they take into account all the wave harmonic components. Time-domain models that do not account for wave memory effects are investigated in Ottosson and Bystrom (1991), Fang et al. (2005), Fossen (2005). Computation of convolution integral is avoided in the above studies because the focus was on regular waves. A similar approach in the time domain is followed in the current work and in Sutulo and Guedes Soares (2008), Sutulo and Soares (2009) to compute regular wave forces acting on the ship.

Apart from the convolution type solutions mentioned above, the manoeuvring characteristics of a ship in waves are also predicted based on a two-time scale approach as given in Skejic and Faltinsen (2008), Yasukawa and Nakayama (2009), Yen et al. (2010), Seo and Kim (2011). Here it is assumed that the high-frequency wave forces affect the seakeeping and the low-frequency drift forces affect the manoeuvring motion. CFD studies Peric and Bertram (2011), Bertram (2012) using finite volume methods come at the cost of higher computational time, which are not helpful for real-time simulations in practice. Experimental studies are carried out on the scaled model of KVLCC2 in Kim et al. (2019) to study the ship's motion in regular waves for a turning circle experiment. For different wave parameters, the effect on drifting distance and angle is studied. Similar experimental studies are carried out in Hasnan et al. (2019) for irregular waves. In Fannemel (2008), Li (2009), the wave loads and moments are calculated using Response Amplitude Operator (RAO) models. These have been deployed in closed-loop simulation studies as external disturbances to study the robustness of controllers.

1.3. Closed-loop control

Open-loop numerical studies can be extended to closed-loop simulations via the inclusion of a control system or autopilot system. PID is a widely used technique for closed-loop control and have evolved over past few decades. Time varying optimal gains (Moradi and Katebi, 2001) and auto tuning fuzzy controller (Tomera, 2017) are examples of how PID controller performance can be improved. In general, however, PID controller pose difficulties in tuning and getting optimal performance.

In this paper, we explore the possibility of using MPC for a ship manoeuvring and path following problem in regular waves and compare its performance with that obtained with a basic PID controller. The states are predicted up to a finite horizon and a cost function is formulated to minimize the deviation from the reference trajectory. The optimal control input is computed subject to dynamics and constraints of the system and the first step of the control input is applied to the system.

MPC owes its popularity to its constraint handling capabilities enabling maximum performance to be extracted when the system is pushed to the operational limits. However, a model predictive controller requires solving a computationally intensive optimization problem at each sampling instant. Depending on the complexity of the model used in the controller, it can result in linear or nonlinear MPC. Linear MPC rely on linear or linearized models of the system dynamics and a Quadratic Program (QP) needs to be solved. A QP is an optimization problem that has a quadratic objective and linear constraints. With advances in numerical computing, QPs can be solved within an order of milliseconds (Kouzoupis et al., 2018). The same does not hold when nonlinear models are used in MPC. Though a nonlinear model provides an accurate representation of the system, the resulting optimization problem is nonlinear and computationally demanding. Moreover, the convexity of the problem is not guaranteed and it is not possible to

predict the runtime bounds of the optimization problem. A line of sight MPC controller is proposed in Oh and Sun (2010) for path following of an underactuated surface vessel. In Zheng et al. (2014) trajectory tracking using linear and nonlinear MPC is performed on a surface vessel in calm water and the accuracy and computational performance of the controllers are compared. A nonlinear model predictive controller is developed in Guerreiro et al. (2014) for trajectory tracking of a catamaran in the presence of constant ocean currents. The error dynamics are derived and saturation constraints for the states and control inputs are imposed using penalty functions to reduce computational time. An equality constrained optimization problem is solved using a gradient-based method. Generally, the wave forces and moments are modelled as external disturbances in closed-loop simulations. Using a response amplitude oscillator, wave disturbances are calculated and the robustness of the controller is studied in the presence of unknown disturbances (Li, 2009). By trial and error, the controller is tuned to avoid infeasibility. In Liu et al. (2011), Li and Sun (2011) a disturbance compensating MPC controller is studied using a disturbance observer.

Though model predictive control is an advanced control technique that explicitly handles constraints on the system, it is computationally demanding to solve an optimization problem at each measurement update. If there is a computational delay, control input based on outdated information of the state is given to the system. This results in a compromise on the closed-loop performance of the controller. Some of the factors affecting the optimization problem's runtime include linear vs nonlinear modelling of the system, fidelity of the model (1 DoF, 2 DoF, ..., 6 DoF) and computing resources availability. A linear model leads to QPs that can be solved using off-the-shelf solvers within the millisecond range. On the other hand, nonlinear models result in a nonlinear optimization problem which is much more challenging to solve in general. Increasing the model fidelity leads to an increase in the number of states and control inputs. This results in a larger dimensional optimization problem for higher fidelity models. Lastly, with advances in numerical computing and hardware architecture, there are powerful single board computers to perform online optimization.

1.4. Scope and objectives

A model predictive control is developed for a unified manoeuvring numerical model, which has never been investigated in the past. In this paper, we consider the ship manoeuvring problem in waves by incorporating both aspects of ship hydrodynamics and control perspective. An autopilot system based on nonlinear MPC (NMPC) is investigated using a unified manoeuvring model. The wave model is incorporated within the system model used by NMPC and control inputs are computed. A 3DoF MMG model is used to represent the dynamics of the ship. Since the ship manoeuvring is limited to the horizontal plane, it is assumed that a 3DoF model will accurately predict the manoeuvring motion. The ship will be subjected to heel during turning. However, the roll motion is neglected here as its inclusion will increase the computational time for the NMPC. The second order mean wave drift forces and moments are computed based on a potential flow method, which provides results that are accurate enough for practical engineering problems. The wave drift forces affect the surge, sway, and yaw motion of the ship. The forces and moments from the propeller, rudder and hydrodynamics are computed using standard methods available in the literature (Yasukawa and Yoshimura, 2015). The standard KVLCC2 tanker model has been used for the simulations.

In the first part of the paper, the 3DoF MMG model is validated for a KVLCC2 tanker by comparing the open-loop simulation results in calm water and in waves with the experimental results available from the literature. In the second part of the paper, a nonlinear MPC controller is used with the 3DoF model for heading control in regular waves for path following using a basic line of sight algorithm. The effectiveness of MPC and PID control are compared for the above path following problem. To improve the computational efficiency of NMPC controller, the necessary derivatives for optimization are computed using automatic differentiation (Griewank and Walther, 2008) and feasibility studies are performed for real-time optimization.

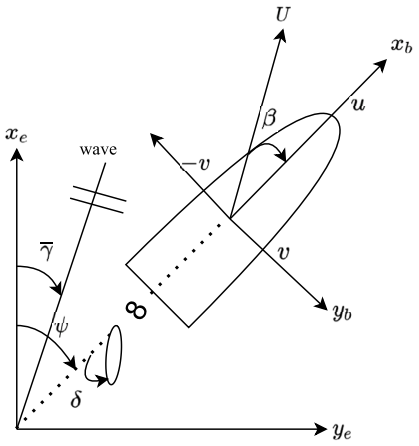

Fig. 1. 3DOF unified model.

The rest of the paper is organized as follows. In Section 2, the dynamics of the unified seakeeping and manoeuvring model is presented. Open-loop simulations in calm water and regular waves are studied in Section 3. In Section 4 the line of sight guidance algorithm is discussed. The definition of the PID and MPC controller, its implementation are discussed in Section 5. The results and discussion of the closed-loop simulations are described in Sections 6–7. Discussions on computational time and conclusions are presented in Sections 8–9.

2. 3DoF unified manoeuvring and seakeeping model

A 3DoF ship model of a KVLCC2 tanker from Yasukawa and Yoshimura (2015) is used to study the manoeuvring of KVLCC2 in regular waves. The degrees of freedom are surge, sway, and yaw, as shown in Fig. 1. The equations of motion are derived in the body reference frame and the coordinate system is given in Fig. 1. (x_e, y_e) and (x, y) denote the inertial/Earth and body reference frames, respectively. The body frame is kept at amidship and the centre of gravity is at $(x_G, 0, 0)$. The linear and angular velocities of the ship in the body reference frame are u, v and r, respectively. The total velocity is given by $U = \sqrt{(u^2 + v^2)}$. x, y are the position coordinates of the ship and ψ, β are the heading and drift/sideslip angles, respectively.m is the ship's mass and $m_{x,y}$ is the added mass component along the respective directions. Similarly, I_{zG}, J_{zG} is the moment of inertia and added moment of inertia about the z-axis, respectively. The waves characterized by frequency ω and height H are defined in the inertial reference frame and it approaches ship at an incidence angle γ as shown in Fig. 1. The wave encounter heading angle χ is defined as the difference of wave incidence and heading angle ($\chi = \gamma - \psi$). X, Y, N are the external sway, surge forces and yaw moments acting on the ship in the body reference frame.

The equations of motion of the 3DoF ship are given in Eq. (1).

$$\begin{aligned}
(m + m_x)\dot{u} - (m + m_y)vr - x_G m r^2 &= X \\
(m + m_y)\dot{v} + (m + m_x)ur + x_G m \dot{r} &= Y \\
(I_{zG} + x_G^2 m + J_Z)\dot{r} + x_G m(\dot{v} + ur) &= N \\
\dot{x_e} &= u\cos\psi - v\sin\psi \\
\dot{y_e} &= u\sin\psi + v\cos\psi \\
\dot{\psi} &= r
\end{aligned} \tag{1}$$

The external forces and moments acting on the ship are composed of contributions from waves (W), hydrodynamic derivatives (H), rudder

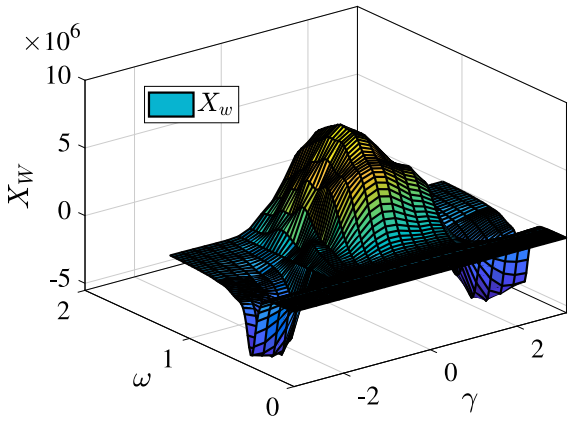

Fig. 2. Interpolation table data for surge wave forces X_w using Salvensen method.

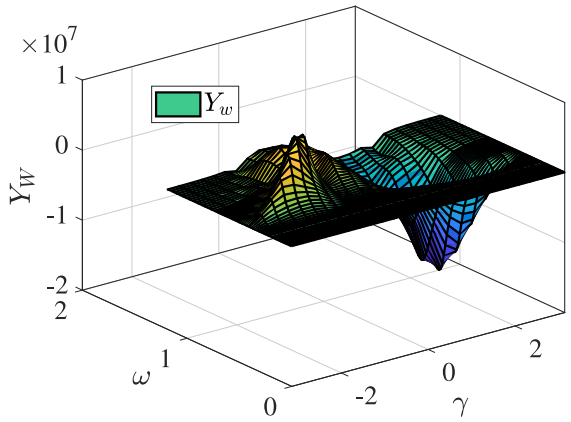

Fig. 3. Interpolation table data for sway wave forces Y_w in using Salvensen method.

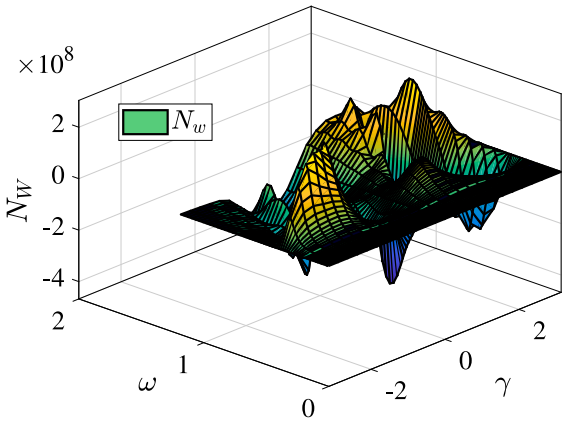

Fig. 4. Interpolation table data for wave yaw moment N_w using Salvensen method.

Table 1
Principal particulars of KVLCC2 tanker.

Particular	Full scale
Length between perpendiculars (m)	320
Breadth (m)	58
Draft (m)	20.8
Displacement Δ(m^3)	312600
mass (kg)	3.12×10^8
I_x(kg m^2)	1.43×10^{11}
I_y(kg m^2)	1.99×10^{12}
I_z(kg m^2)	1.99×10^{12}
Longitudinal centre of gravity X_G (m)	11.2
Block coefficient C_b	0.810
Propeller dia. D_p (m)	9.86
Rudder height H_R (m)	15.80
Rudder Area A_R (m^2)	112.5

(R) and propeller (P).

$$X = X_W + X_H + X_R + X_P \tag{2}$$

$$Y = Y_W + Y_H + Y_R \tag{3}$$

$$N = N_W + N_H + N_R \tag{4}$$

The hydrodynamic derivatives, the propeller thrust, rudder forces and moments are calculated based on Yasukawa and Yoshimura (2015).

2.1. 2nd order wave loads

A two-time scale approach is followed in this paper for studying the manoeuvring motions in waves. It is assumed that the manoeuvring motions are affected by the low-frequency wave responses and the seakeeping by high-frequency responses. Therefore, second order mean drift forces are calculated based on the method proposed by Salvesen (1974). The longitudinal and lateral drift forces and the 2nd order yaw moments are pre-calculated for a range of frequency and heading. During the manoeuvring simulations, the encountering wave heading with respect to the ship's x-axis changes. The drift forces/moments are interpolated for the corresponding wave heading for each time step using bsplines. The longitudinal, lateral drift forces and the yaw for a range of wave heading between −180 deg to 180 deg and frequency are shown in Figs. 2–4. The method used in Salvesen (1974) is not suitable for the calculation of 2nd order wave loads in shorter waves, particularly for a wave to ship length ratio equal to or less than 0.5. Therefore in this study, the manoeuvring motions are limited to wave to ship length ratio greater than 0.7.

In Table 1, the ship particulars for the KVLCC2 tanker are listed. Further information regarding the values of hydrodynamic hull derivatives, resistance and propeller characteristics etc., can be found in Yasukawa and Yoshimura (2015).

2.2. Nonlinear state space

The dynamics of the ship can be written in state-space form as a set of differential equations involving the state ($\bar{x}$) and control input ($\bar{u}$) vector as follows,

$$\frac{d}{dt}\bar{x} = \begin{bmatrix} \dot{u} \\ \dot{v} \\ \dot{r} \\ \dot{x} \\ \dot{y} \\ \dot{\psi} \end{bmatrix} = f(\bar{x}, \bar{u}) = \begin{bmatrix} A^{-1} b_1 \\ b_2 \end{bmatrix}$$

$$A = \begin{bmatrix} (m + m_x) & 0 & 0 \\ 0 & (m + m_y) & x_G m \\ 0 & x_G m & (I_{zG} + x_G^2 m + J_Z) \end{bmatrix} \tag{5}$$

$$b_1 = \begin{bmatrix} X + (m + m_y) v r + x_G m r^2 \\ Y - (m + m_x) u r \\ N - x_G m u r \end{bmatrix}, \quad b_2 = \begin{bmatrix} u \cos\psi - v \sin\psi \\ u \sin\psi + v \cos\psi \\ r \end{bmatrix}$$

where $\bar{x} = [u\ v\ r\ x\ y\ \psi]^T$ is the state vector and $\bar{u} = [n_P\ \delta]^T$ is the control input vector.

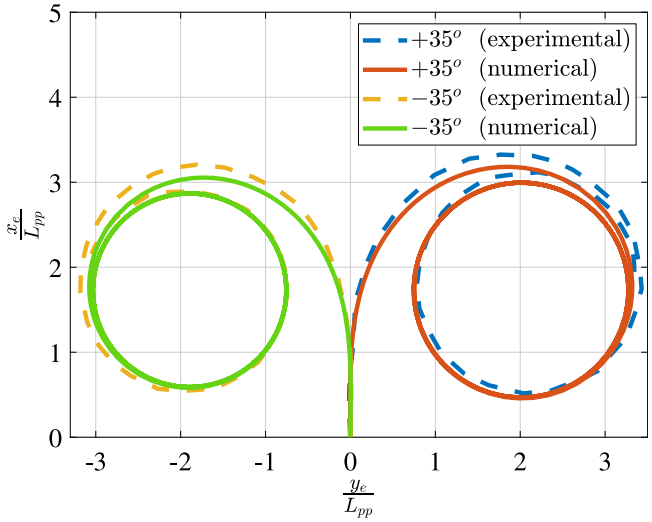

Fig. 5. Calm water results comparison with Yasukawa and Yoshimura (2015).

Table 2
Calm water turning circle parameter comparison with Yasukawa and Yoshimura(2015) (Yasukawa and Yoshimura, 2015).

Particulars	Advance	Tactical Dia.	Transfer
Simulation ($\delta = -35$deg)	3.18	3.11	1.8
Yasukawa and Yoshimura (2015)	3.11	3.08	1.95
Simulation ($\delta = 35$deg)	3.30	3.17	1.67
Yasukawa and Yoshimura (2015)	3.25	3.34	1.7
Avg. accuracy (%)	98.1	97	95.32

3. Open loop simulations in calm water and waves

3.1. Calm water

Numerical simulation using the 3DoF model is performed in calm water for the KVLCC2 tanker for 35 deg starboard and port side turn. The ship's steady-state surge velocity is set to 8 ms^{-1} and the steady-state RPS is 1.783 corresponding to the experimental condition (Kim et al., 2019). With the remainder of states set to zero at $t = 0$, a constant rudder deflection of ± 35 deg is applied throughout the simulation. The numerical simulation results are compared with the experimental results provided in Yasukawa and Yoshimura (2015). As inferred from Fig. 5, the numerical and experimental results are in close agreement with each other for the starboard and port side turn.

Table 2 compares the calm water turning circle parameters with the experimental results from Yasukawa and Yoshimura (2015). The advance, tactical diameter and the transfer of the vessel are compared. For all three cases, the percentage of error is less than 5% for both port and starboard turn.

3.2. Waves

Prior to closed-loop simulation in the presence of waves, the accuracy of wave forces and moments modelling is evaluated by conducting open-loop simulations in waves. The manoeuvring characteristics of the KVLCC2 tanker are simulated in regular waves. Head and beam wave conditions are used for simulations, where the wave frequency is set to 0.439 rad s^{-1}, which corresponds to a wave to ship length ratio, λ/L_{pp}, of 1, and the wave steepness ($\frac{H}{\lambda}$) corresponding to a value of 0.02 is used. During the simulation, the Froude number F_n is set to a constant value of 0.142, which corresponds to a ship forward speed of 8 ms^{-1}. In addition to $\lambda/L_{pp} = 1$, the open-loop trajectory in head waves are also numerically simulated for $\lambda/L_{pp} = 0.7, 1.2$ and 1.5.

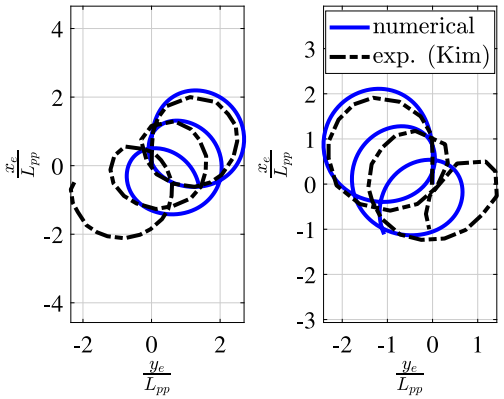

Fig. 6. Comparison of turning circle trajectory in head waves for $\frac{\lambda}{L_{pp}} = 1$ with the experimental trajectory.

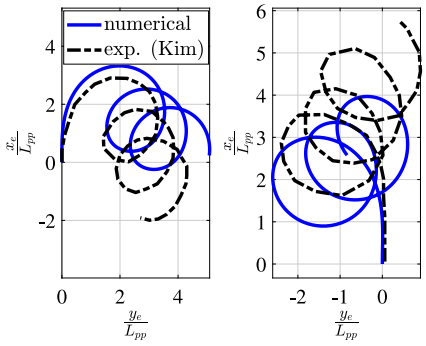

Fig. 7. Comparison of turning circle trajectory in beam waves for $\frac{\lambda}{L_{pp}} = 1$ with the experimental trajectory.

Kim et al. (2019) performed experiments for a KVLCC2 tanker in regular waves. The trajectory data from the experiments are collected and it is used as a baseline to validate wave force and moment model. The propeller's RPS is set to 1.783 and the initial conditions used for the state is taken from Kim et al. (2019). The trajectory obtained from the simulations for head and beam waves for $\lambda/L_{pp} = 1$ is given in Figs. 6–7. It is compared with the trajectory obtained from the experiment. The ship's drifting nature in head and beam waves is in agreement with the results obtained from the experiments. However, an exact match between the trajectories is not observed. One of the reasons can be due to the 2D assumption and other limitations of the strip theory based drift force calculation method.

It can be seen that ship trajectory is not symmetric while taking port and starboard turn. This asymmetry is due to flow straightening effect. When a ship takes a turn, the inflow angle to the rudder will be reduced than the geometric inflow angle. However, the flow straightening effect due to the presence of the hull and propeller slip stream improves the inflow angle to the rudder (Yasukawa and Yoshimura, 2015; Molland and Turnock, 2002). The flow straightening coefficient γ_R takes different values for port and starboard turning and this results in the asymmetry in the port and starboard side turning. For KVLCC2 tanker, the γ_R values are 0.395 and 0.640, respectively, when effective inflow angles to the rudder are lesser and greater than 0.

Fig. 8 compares the numerical and experimental trajectory in regular waves with a wave to ship length ratio equal to (a) 0.7 (b) 1.2 and (c) 1.5, respectively.

In order to quantify the accuracy of the numerical prediction, drifting distance and drifting angles are compared. Fig. 9 illustrates the estimation of the drifting distances and angles in waves. A drifting

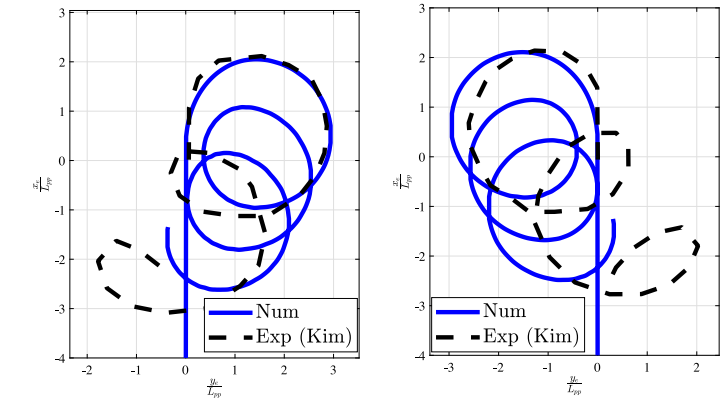

(a) $\lambda/L_{PP} = 0.7$

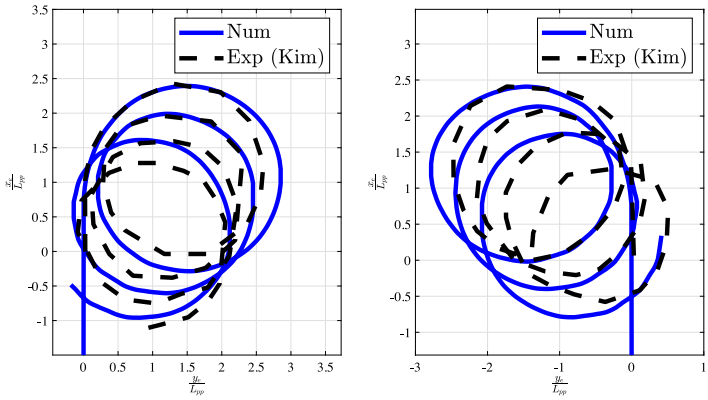

(b) $\lambda/L_{PP} = 1.2$

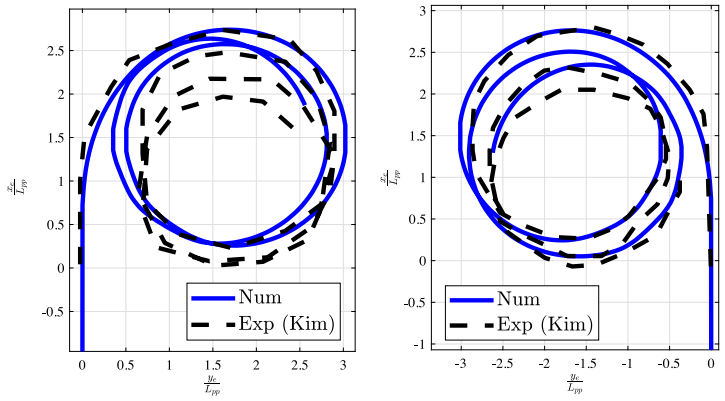

(c) $\lambda/L_{PP} = 1.5$

Fig. 8. Comparison of turning circle trajectory in head waves for different wave to ship length ratio with the experimental trajectory from Kim et al. (2019).

Table 3
Comparison of drifting distance in head seas for a range of wave to ship length ratio.

δ(deg)	Wave heading (deg)	H/L_{pp}	λ/L_{pp}	$D_{dr90-450}$		$D_{dr180-540}$		$D_{dr270-630}$	
				Num.	Exp.	Num.	Exp.	Num.	Exp.
35	180	0.02	0.7	0.96	2.03	0.98	2.26	0.91	2.16
			1	1.25	0.97	1.18	1.11	1.19	1.10
			1.2	0.42	0.36	0.49	0.41	0.47	0.35
			1.5	0.16	0.44	0.23	0.37	0.17	0.28

distance of 180–540, $D_{dr180-540}$, shows the parallel drifting distance between two heading angles, i.e. 180 and 540 degrees. Similarly, the drifting angle is the angle between the line representing drifting distance and the inertial X-axis. The differences in head waves are quantified by comparing the drifting distance and angles as given in Tables 3 and 4.

The experimental drifting distances decrease as the wavelength increases. The same trend is followed in the numerical simulation except for the highest frequency, i.e. for $\lambda/L = 0.7$. This could be due

Table 4
Comparison of drifting angle in head seas for a range of wave to ship length ratio.

δ(deg)	wave heading (deg)	H/L_{pp}	λ/L_{pp}	$A_{dr90-450}$		$A_{dr180-540}$		$A_{dr270-630}$	
				Num.	Exp.	Num.	Exp.	Num.	Exp.
35	180	0.02	0.7	175	154	156	147	157	148
			1	120	135	128	125	115	128
			1.2	158	160	127	146	132	143
			1.5	186	224	115	182	79	152

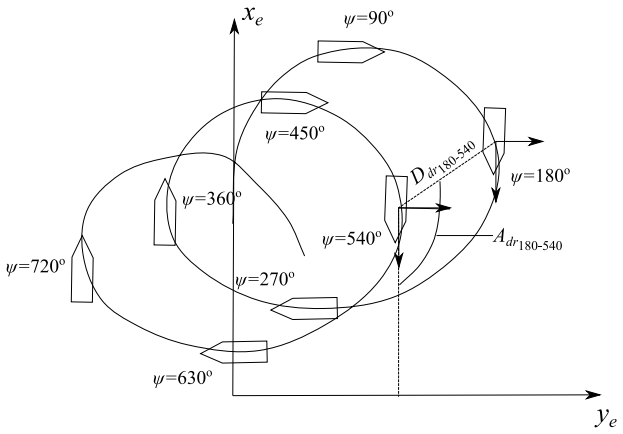

Fig. 9. Pictorial illustration of the drifting distance and drifting angle..

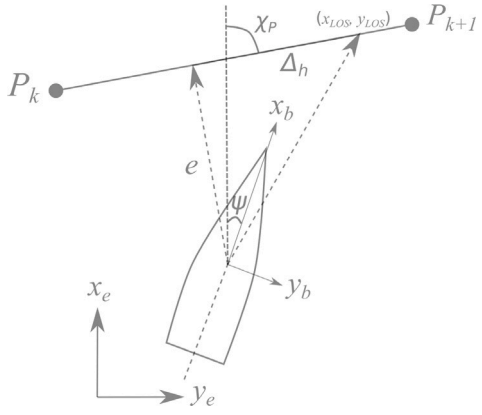

Fig. 10. Line of Sight illustration.

to the limitations of the Salvesen (Salvesen, 1974) method which is suitable for longer waves. The ship experiences the maximum drifting angle in the longest waves, i.e. for $\lambda/L = 1.5$ in both the numerical and experimental simulations. For the simulations in $\lambda/L = 1.0$, which is used in the following sections for closed-loop simulation, the error in the estimation of the drifting distance is less than 10% except for the first drifting distance, i.e. $D_{dr90-450}$. Similarly, the error in the estimation of the drifting angle is approx.10%.

4. Waypoint navigation using LOS guidance

A popular algorithm for path following is the line of sight (LOS) (Lekkas and Fossen, 2013) algorithm. In Fig. 10, some of the main variables used in the LOS algorithm are indicated. The desired heading ψ_d is calculated based on Eq. (6)

$$\psi_d = \chi_p + arctan(-e/\Delta_h) - \beta \tag{6}$$

where Δ_h is the look ahead distance, e is the cross track error, β is the drift angle and χ_p is the horizontal path-tangential angle.

5. Closed-loop simulations

Based on the desired heading calculated from the LOS algorithm, the controller computes the necessary control input to the ship to track the desired heading angle. Here the ship is further underactuated by setting the speed of the propeller to a constant value. Hence, the rudder deflection is only available to control the ship. This paper uses a nonlinear MPC and PID controller as depicted in the respective block diagrams in Fig. 11.

5.1. PID

Proportional Integral Derivative (PID) control is a feedback control algorithm widely used in industries for SISO systems. Here we use a simple PID control for a comparison with the results generated using MPC. The error between the setpoint to be tracked and the current measurement is computed using the control law.

$$u_{PID}(t) = K_p\bar{e}(t) + K_d\frac{d\bar{e}(t)}{dt} + K_i\int_0^t \bar{e}(\tau)d\tau, \quad \bar{e}(t) = \psi_d - \psi(t) \tag{7}$$

The gains K_p, K_i, K_d can be tuned appropriately to meet requirements like maximum overshoot, settling and rise time. System identification is performed using simulation data from the turning trajectory of the 3DOF model to obtain parameters of the first-order Nomoto model. The resulting first-order model is given in Eq. (8).

$$26.15\dot{r} + r = 0.0132\delta \tag{8}$$

The PID tuner available in MATLAB is used with the identified Nomoto model to obtain initial gain estimates. Further, fine-tuning using trial-error is performed in closed-loop simulation to fix the values for the gains K_p, K_i, K_d given in Eq. (9).

$$K_p = 17, \quad K_i = 15, \quad K_d = 0.2285 \tag{9}$$

For aggressive control, large gains for PID controller can be chosen but they often tend to get clipped by the saturation block, and the stability of the controller is not guaranteed without proper anti-windup techniques. For MIMO systems, the dynamics are often coupled and synthesis PID control laws become tedious. Moreover, frequent tuning is required to perform well with varying operating conditions.

Though methods based on adaptive tuning of PID gains are available, the study here is limited to a simple and basic PID controller for the purpose of comparison.

5.2. Nonlinear MPC (NMPC)

Many issues prevalent in PID based systems can be overcome by means of using model predictive control. Also known as receding horizon control, the control input is computed by means of solving a constrained optimization problem online where model dynamics and operational limits are explicitly taken into consideration. The development time is much shorter and model changes or inclusion of performance constraints can be performed on the fly unlike PID where a complete redesign of the controller maybe required.

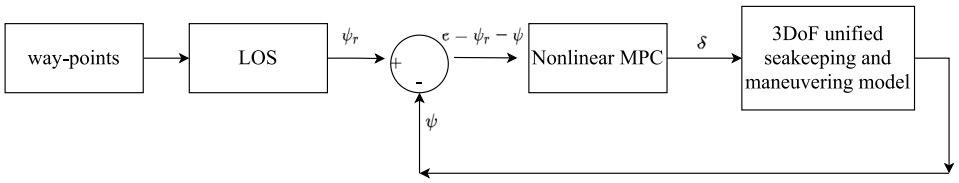

(a) Nonlinear MPC

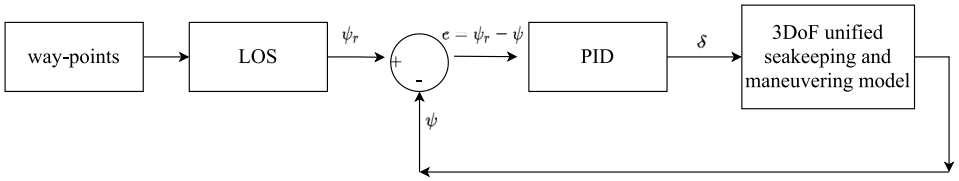

(b) PID

Fig. 11. Nonlinear MPC and PID block diagram.

Nonlinear MPC (Rawlings et al., 2017) for the unified manoeuvring model in continuous-time is based on repeatedly solving a finite-horizon optimal control problem at each measurement update given by Eq. (10)

$$\begin{aligned} \min_{\bar{x},\bar{u}} \quad & \int_0^{T_P} \left(\left\| \bar{x} - \bar{x}_r \right\|_Q^2 + \left\| \bar{u} - \bar{u}_r \right\|_R^2 \right) dt + \left\| (\bar{x}(T_P) - \bar{x}_r(T_P)) \right\|_S^2 \\ \text{s.t.} \quad & \bar{x}(0) = \hat{x} \\ & \dot{\bar{x}} = f(\bar{x}, \bar{u}) \\ & \bar{u}_- \le \bar{u} \le \bar{u}_+ \\ & \bar{x}_- \le \bar{x} \le \bar{x}_+ \forall t \in [0, T_P] \end{aligned} \tag{10}$$

where $\|(*)\|_Q^2 = (*)^T Q(*)$ and T_P denotes the prediction horizon of nonlinear MPC. The integral represents the weighted least squared cost function, which penalizes the deviation of the state and control inputs from their reference trajectories, $\bar{x}_r$ and $\bar{u}_r$ respectively. The Mayer term $(\|(\bar{x}(T_P) - \bar{x}_r(T_P))\|_S^2)$ also known as cost-to-go or terminal cost in the context of nonlinear MPC is often included for closed-loop stability. For trajectory tracking applications, the weighting matrices Q, R, S are chosen as positive semi-definite matrices.

The equality constraint, $\dot{\bar{x}} = f(\bar{x}, \bar{u})$ represents the dynamics of the unified manoeuvring model using the differential equations given in Eq. (5). The upper $(\bar{x}_+, \bar{u}_+)$ and lower bounds $(\bar{x}_-, \bar{u}_-)$ on the state and control variables are imposed as inequality constraints on $\bar{x}$ and $\bar{u}$. At each time instant, a measurement of the state $\hat{x}$ is assumed to be available and the optimal control problem is solved. The first optimal control input is applied to the system and the process repeats until the tracking error goes to zero. The main advantage of MPC is that control inputs which are feasible with respect to dynamics and constrained are given to the system. In addition, in the present study the effect of wave forces in unified manoeuvring model is accounted during optimization which leads to better control actions.

The continuous-time optimal control problem given in Eq. (10) is numerically solved using trapezoidal collocation which transforms the optimal control problem to a finite-dimensional optimization problem. The control input and the state trajectory are approximated using a piecewise constant and linear polynomial respectively in trapezoidal collocation on a uniform grid with the discrete time t_k defined as follows

$$t_k = (k-1)\Delta t, \quad \Delta t = T_P / N, \quad k = \{1, 2, \ldots, N+1\} \tag{11}$$

The discrete states and controls are $\bar{x}_1, \ldots, \bar{x}_{N+1}$ and $\bar{u}_1, \ldots, \bar{u}_N$ respectively. The trapezoidal collocation of the dynamics results in the discrete dynamics equation. The integral is approximated using a rectangle rule and the inequality constraints corresponding to the bounds on the state and control variables are evaluated at the node points t_k. The resulting discrete optimal control problem/ nonlinear optimization problem is given in (12).

$$\begin{aligned} \min_{\bar{x}_1, \bar{x}_2, \ldots, \bar{u}_N} \quad & \sum_{k=1}^{N} \left(\left\| \bar{x}_k - \bar{x}_r \right\|_Q^2 + \left\| \bar{u}_k - \bar{u}_r \right\|_R^2 \right) \Delta t + \left\| (\bar{x}_{N+1} - \bar{x}_{r,N+1}) \right\|_S^2 \\ \text{s.t.} \quad & \bar{x}_1 = \hat{x} \\ & \bar{x}_k = \bar{x}_{k-1} + \frac{\Delta t}{2} (f(\bar{x}_{k-1}, \bar{u}_{k-1}) + f(\bar{x}_k, \bar{u}_{k-1})) \\ & \bar{u}_- \le \bar{u}_k \le \bar{u}_+ \\ & \bar{x}_- \le \bar{x}_k \le \bar{x}_+ \end{aligned} \tag{12}$$

Table 5
MPC controller parameters.

Parameter	Value
T_s	1
T_P	5
Q	diag([0 0 0 0 0 100])
R	diag([10^{-2} 10])
S	diag([0 0 0 0 0 1000])

Table 6
Bounds.

State/Control input	Lower bound $((*)_-)$	Upper bound $((*)_+)$
u	0	20
v	−5	5
r	−1	1
n_p	1.783	1.783
δ	$-35\pi/180$	$35\pi/180$

The sampling time, prediction horizon and weighting matrices are provided in Table 5 and the upper and lower limits of state and control variables are given in Table 6. The desired heading from the LOS algorithm is the output to be tracked and the rudder angle is varied to adjust the course. This is accounted in the weighting matrix Q and constant propeller speed is imposed using equal lower and upper bounds in the optimization problem as shown in Tables 5–6. In the optimization problem the position and heading angles are not constrained, however from a numerical perspective it is not possible to set infinite bounds and the absolute values of these variables are bounded by a large number (10^6).

5.3. Nonlinear optimization

The discrete NMPC problem from Eq. (12) can be expressed in a standard nonlinear optimization form as shown in Eq. (13). F is the

objective function and G, H are equality and inequality constraint vector, respectively. W is the decision variable vector consisting of the discrete state and control inputs. The definitions of the functions F, G, H are provided in Eqs. (15)–(18). The equality constraint vector $G(W)$ consists of the initial condition on the state and the discrete dynamics equations. Similarly, the upper and lower bound on discrete state and control variable at each node point is stacked in the inequality constraint vector $H(W)$.

$$\begin{aligned} \min_{W} \quad & F(W) \\ \text{s.t.} \quad & G(W) = 0 \\ & H(W) \leq 0 \end{aligned} \tag{13}$$

$$W = \begin{bmatrix} \bar{X} \\ \bar{U} \end{bmatrix}, \quad \bar{X} = \begin{bmatrix} \bar{x}_1 \\ \vdots \\ \bar{x}_{N+1} \end{bmatrix}, \quad \bar{U} = \begin{bmatrix} \bar{u}_1 \\ \vdots \\ \bar{u}_N \end{bmatrix}$$

$$F(W) = (W - W_r)^T \begin{bmatrix} \hat{Q} & 0 \\ 0 & \hat{R} \end{bmatrix} (W - W_r) \tag{14}$$

$$\hat{Q} = \begin{bmatrix} Q\Delta t & \dots & 0 \\ 0 & \ddots & 0 \\ 0 & 0 & Q\Delta t + S \end{bmatrix}, \quad \hat{R} = \begin{bmatrix} R\Delta t & \dots & 0 \\ 0 & \ddots & 0 \\ 0 & 0 & R\Delta t \end{bmatrix} \tag{15}$$

$$G(W) = \begin{bmatrix} \bar{x}_1 - \hat{x} \\ \bar{x}_2 - \bar{x}_1 - \frac{\Delta t}{2}(f(\bar{x}_1, \bar{u}_1) + f(\bar{x}_2, \bar{u}_1)) \\ \bar{x}_3 - \bar{x}_2 - \frac{\Delta t}{2}(f(\bar{x}_2, \bar{u}_2) + f(\bar{x}_3, \bar{u}_2)) \\ \vdots \\ \bar{x}_{N+1} - \bar{x}_N - \frac{\Delta t}{2}(f(\bar{x}_N, \bar{u}_N) + f(\bar{x}_{N+1}, \bar{u}_N)) \end{bmatrix}, \tag{16}$$

$$H(W) = \begin{bmatrix} \bar{x}_1 - \bar{x}_+ \\ \bar{x}_2 - \bar{x}_+ \\ \vdots \\ \bar{x}_{N+1} - \bar{x}_+ \\ -\bar{x}_1 + \bar{x}_- \\ -\bar{x}_2 + \bar{x}_- \\ \vdots \\ -\bar{x}_{N+1} + \bar{x}_- \\ \bar{u}_1 - \bar{u}_+ \\ \bar{u}_2 - \bar{u}_+ \\ \vdots \\ \bar{u}_N - \bar{u}_+ \\ -\bar{u}_1 + \bar{u}_- \\ -\bar{u}_2 + \bar{u}_- \\ \vdots \\ -\bar{u}_N + \bar{u}_- \end{bmatrix} \tag{17}$$

$$\bar{x}_- = \begin{bmatrix} 0 \\ -5 \\ -1 \\ -10^6 \\ -10^6 \\ -10^6 \end{bmatrix}, \quad \bar{x}_+ = \begin{bmatrix} 20 \\ 5 \\ 1 \\ 10^6 \\ 10^6 \\ 10^6 \end{bmatrix}, \quad \bar{u}_- = \begin{bmatrix} 1.783 \\ -35\frac{\pi}{180} \end{bmatrix}, \quad \bar{u}_+ = \begin{bmatrix} 1.783 \\ 35\frac{\pi}{180} \end{bmatrix} \tag{18}$$

Trapezoidal collocation results in optimization problems which are large yet sparse in nature. To efficiently solve the optimization problem, the gradient, Jacobian and Hessian required for optimization are computed using automatic differentiation (Griewank and Walther, 2008) and the open-source solver IPOPT (Wächter and Biegler, 2006) is used. IPOPT uses an interior-point algorithm for solving large and sparse nonlinear optimization problems.

Computing the gradient of the objective function, Jacobian of the constraints and Hessian of the objective are critical components of numerical optimization algorithm. Ideally, analytical derivatives are the most efficient and accurate, however hand coded derivatives are prone to errors and cumbersome for large and complex problems. A widely used method to compute derivatives is finite-difference method due to ease of implementation but they are prone to approximation and truncation errors. Optimization problems arising from nonlinear MPC have a sparse structure which can be exploited by using state of the art methods like automatic differentiation (Griewank and Walther, 2008). An expression graph for a computer function is created and a chain rule is applied to differentiate the expressions. Based on differentiation rules, a computer function to evaluate the derivatives is constructed. The derivatives computed using automatic differentiation are accurate up to machine precision and by exploiting sparsity they are efficiently computed. The computational complexity of computing the gradient of a function with n inputs via classical finite difference is approximately $(n + 1)$ times the cost of evaluating the function. On the other hand, automatic differentiation can achieve the same with higher accuracy with a complexity of evaluation almost same as that of the function itself and independent of n. Non-smooth functions in optimization can lead to numerical issues and hamper convergence of the optimization algorithm. The flow straightening coefficient given in Yasukawa and Yoshimura (2015)

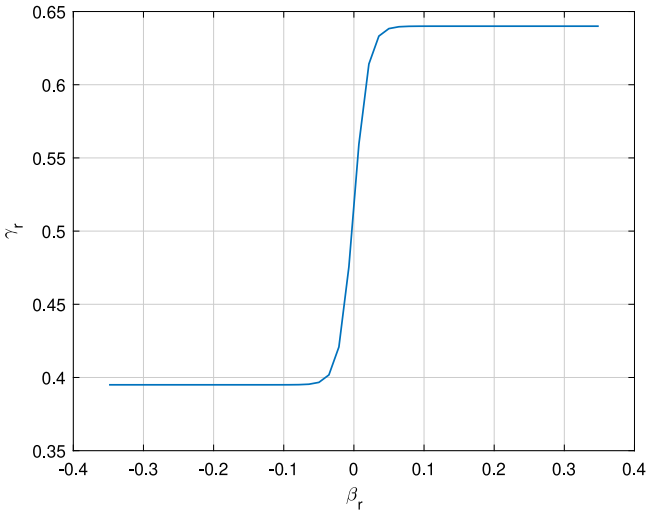

Fig. 12. Approximation of γ_r.

$$\gamma_r(\beta_r) = \begin{cases} 0.395 & \beta_r \leq 0 \\ 0.64 & \beta_r > 0 \end{cases} \tag{19}$$

is a non-smooth function of effective inflow angle to the rudder (β_r). Such non-smooth functions with conditional statements are not well-handled by automatic differentiation. Hence, a smooth approximation of Eq. (19) using tanh function is constructed as follows(see Fig. 12).

$$\gamma_r = \frac{(0.64 - 0.395)}{2} \tanh(50\beta_r) + \frac{(0.64 + 0.395)}{2} \tag{20}$$

Derivatives required for solving nonlinear MPC are computed via automatic differentiation using casADi (Andersson et al., 2019) software. For faster evaluation, the codes for the function and their derivatives are parallelized using `OpenMP` (Dagum and Menon, 1998) and C-code generation is performed. The resulting C-codes are called from MATLAB using MEX files.

6. Manoeuvring and control of a ship in calm water

The path following problem using PID and MPC controllers is investigated in this section. Throughout the simulations, the propeller speed is set to a constant value of 1.783 RPS. Waypoints from Table 7 are used and simulations are carried out using PID and MPC controller. The given waypoints are chosen so that they represent a tighter trajectory which helps to look at the controller performance in a confined space. The results are presented in Figs. 13–17. The MPC and PID controllers are able to follow the desired trajectory in calm water successfully. The rudder deflection and their rates are constrained within limits specified.

Table 7
Waypoints.

$\frac{x}{L_{PP}}$	$\frac{y}{L_{PP}}$
−1.0000	0
0	0
1.3715	0.0006
3.4528	0.2405
5.3252	1.1186
6.7137	2.8690
7.0699	4.7973
6.4006	6.9024
4.9725	8.2881
2.9001	8.8963
0.8873	8.4753
−0.7203	7.1546
−1.5384	5.1716
−1.3605	3.1896
−0.1359	1.3231

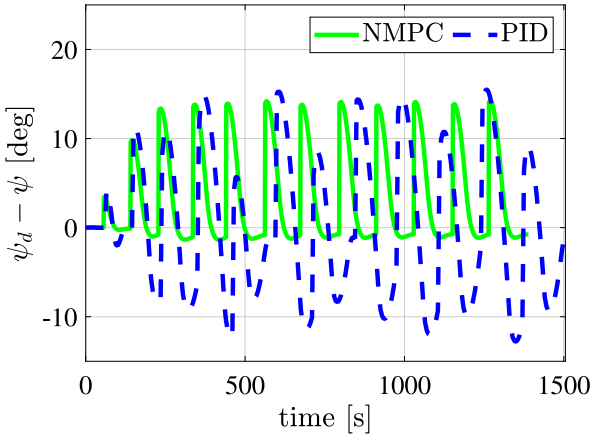

Fig. 13. Error in heading angle.

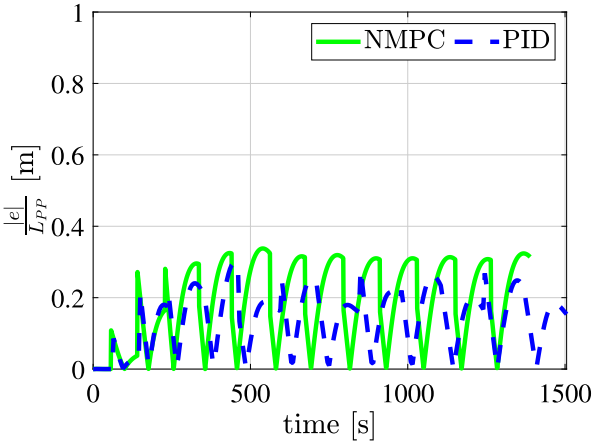

Fig. 14. Cross track error magnitude.

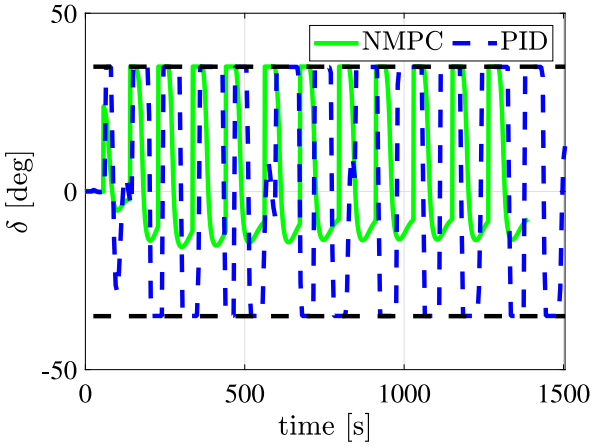

Fig. 15. Rudder deflection.

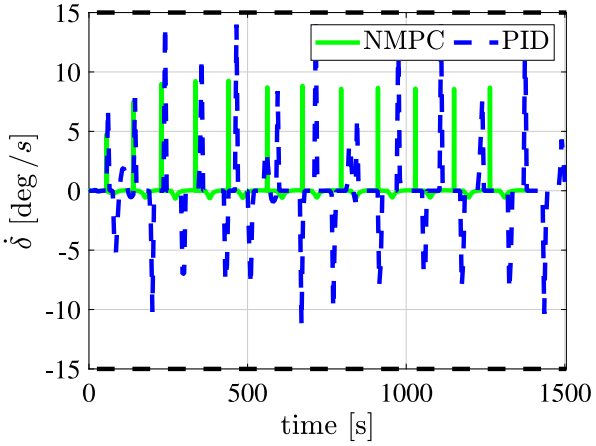

Fig. 16. Rudder deflection rate.

The saturation of control input is lower for MPC in comparison to the PID controller. As a result, smaller and decaying oscillation in error between the heading angles is observed and nonlinear MPC is able to achieve the task in a shorter amount of time. The magnitude of cross-track error is comparable for both the controllers. Large oscillations in the heading error angle are due to a sudden change in reference heading angle when waypoints are switched. This may not be the case if waypoints are well spaced. Here, waypoints are chosen for tighter turns in limited space environment like a harbour. They can be further improved by choosing other path following algorithms that can explicitly take into account the curvature of the path to be followed. Moreover, ships with large block coefficient values like tankers are designed for better directional stability, which reduces the manoeuvring characteristics.

7. Manoeuvring and control of ship in waves

The path following characteristics of the tanker in head and beam waves for a $\lambda/L_{pp} = 1$ and $H/\lambda = 0.02$) is investigated here. For head and beam wave sea conditions, the ship was observed to drift away from its path. The deviations from the course are corrected using a nonlinear model predictive and PID controller for head and beam wave conditions. Using the unified sea keeping and manoeuvring model, the closed-loop simulations are performed and the results are given in Figs. 18–27. MPC and PID track the desired path satisfactorily. Compared to the results from calm water simulations, the error in heading and cross-track error are larger in magnitude in the presence of waves conforms to expectations. The rudder deflection and rates are within limits specified for the controller. Nonlinear MPC is able to track the path in a shorter amount of time in comparison to PID. The deviation from the path is high at two instances in time for beam and head conditions. The waves generate large drift forces in sway and yaw moment. Due to the rudder's inability to counter the forces and moments (saturation limits on deflection and rates), larger deviations are observed. Nonlinear MPC uses lower control effort than the PID controller and this could lower the energy that needs to be spent to actuate the rudder. The cross track error goes up to 0.6 times the

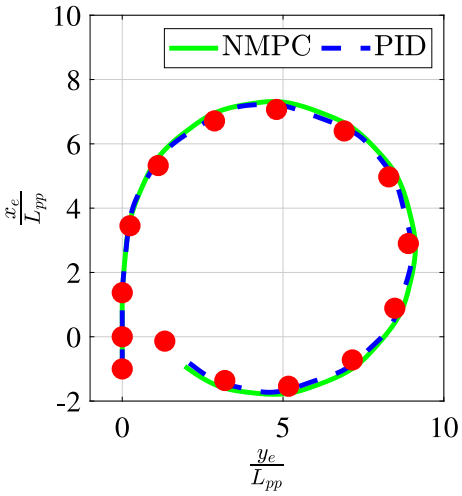

Fig. 17. Path following.

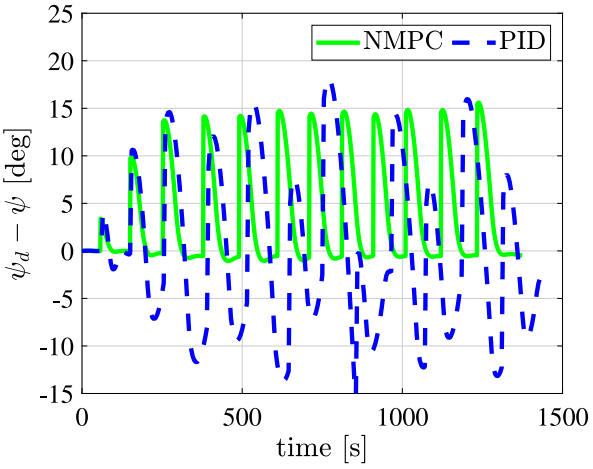

Fig. 18. Error in heading angle (head waves).

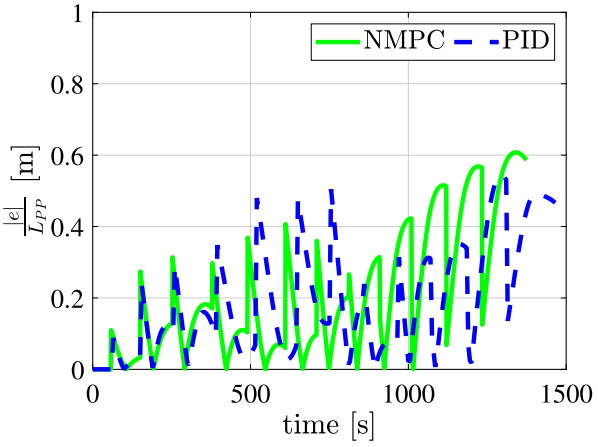

Fig. 19. Cross track error magnitude (head waves).

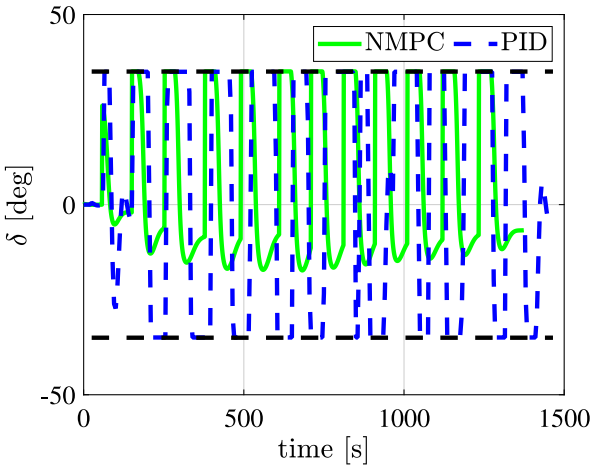

Fig. 20. Rudder deflection (head waves).

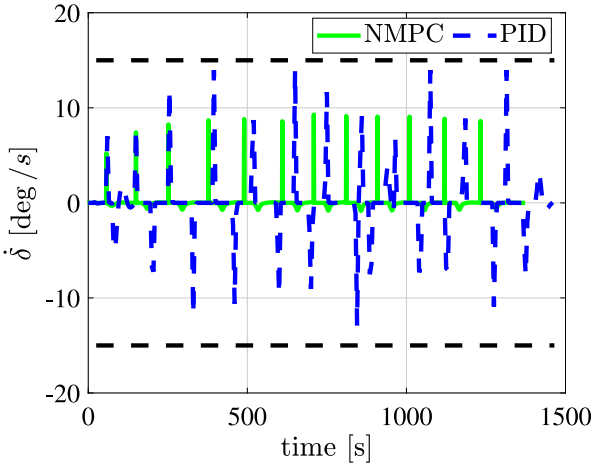

Fig. 21. Rudder deflection rate (head waves).

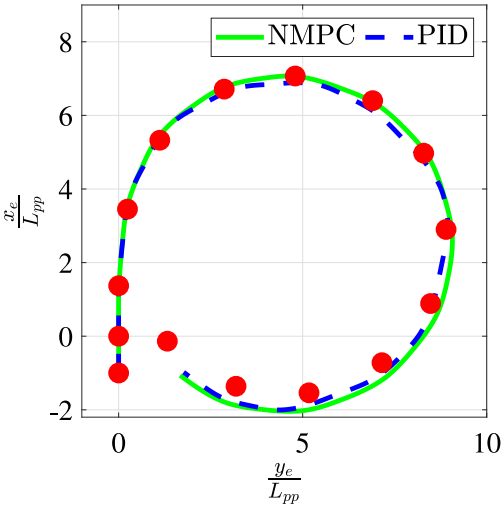

Fig. 22. Path following (head waves).

ship length. As mentioned above in Section 6, this may be due the inability of the LOS algorithm to facilitate a smooth transition while switching between two path segments defined by the ways point, or a tight selected trajectory, or the characteristics of the ship hull.

For a specific wave condition, the closed-loop simulations with two different controllers are performed. If the wave parameters such as steepness and frequency are varied, the controller needs to be manually tuned to cope with the changing wave conditions. This is true for

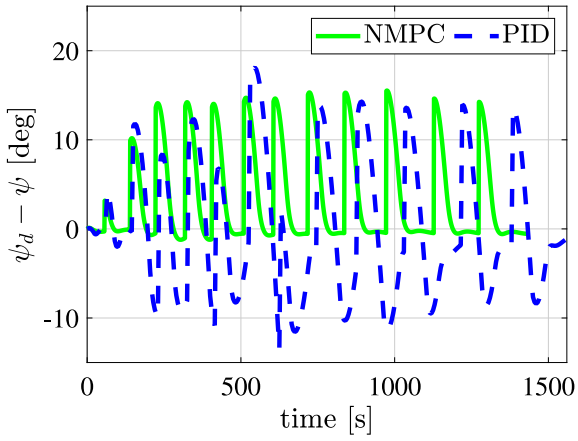

Fig. 23. Error in heading angle (beam waves).

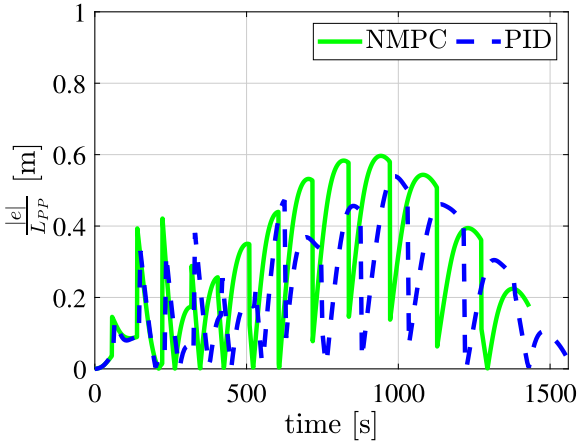

Fig. 24. Cross track error magnitude (beam waves).

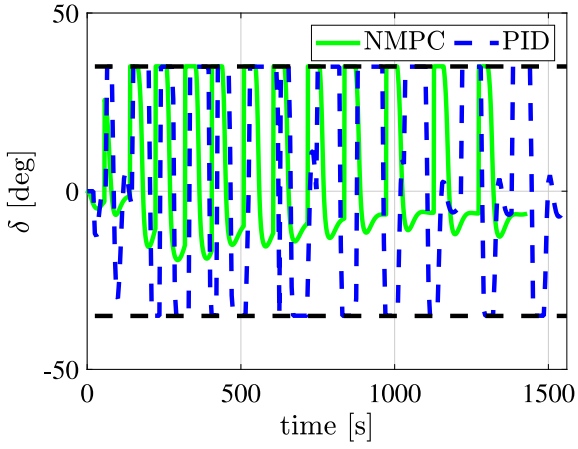

Fig. 25. Rudder deflection (beam waves).

the PID controller and it requires manual tuning for each sea state. Nonlinear MPC controller does not require such tuning and adapts to the changes through the model.

In order to understand the robustness of the controller, the path following simulations are conducted in regular waves of high amplitude using the same settings for each of the controllers. Here, waves with an amplitude of 9 m and frequency of 0.439 rad are chosen, i.e. a wave steepness of $H/\lambda = 0.05$. The waypoints for the path following

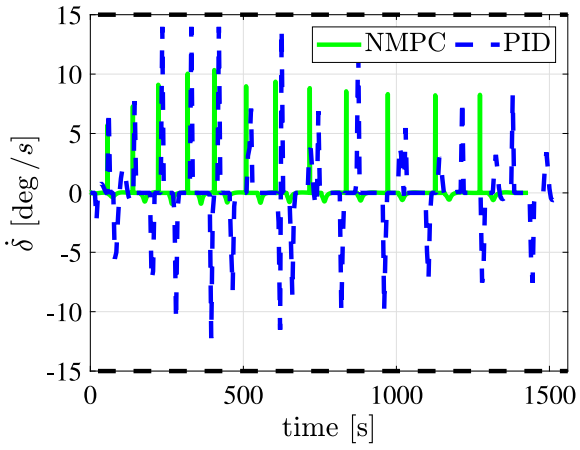

Fig. 26. Rudder deflection rate (beam waves).

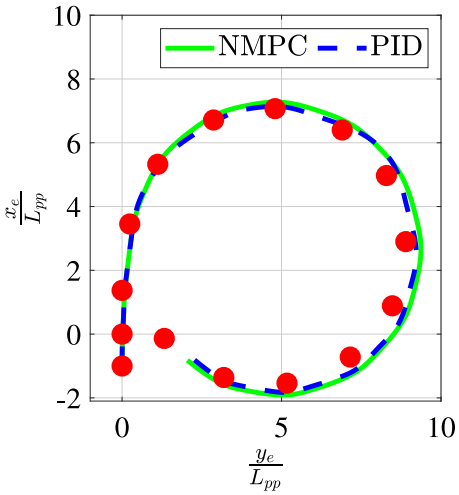

Fig. 27. Path following (beam waves).

are marked in Fig. 31. The results from the simulations are given in Figs. 28–34. Without additional tuning, it is observed that the performance of the PID controller is poor. A large error in heading and cross-track error is observed for PID and for the most part, the rudder remains saturated. This leads to large oscillations in the heading angle of the ship. In response, the ship's forward speed is reduced and oscillations in sway velocity can be observed. As a result, the ship with a PID controller takes a larger amount of time to reach the final waypoint. In contrast, even without tuning the parameters of the NMPC controller, it results in better path following. NMPC controller is able to steer the ship to the desired heading angle and results in lower cross-track error compared to PID. The cross-track error settles to a value of 80 m for NMPC even though the error between the heading angle is driven to zero. This is likely due to the of effect of wave disturbances not considered in the LOS algorithm and a small offset in the rudder deflection can also be observed. This can be overcome by including the effect of the disturbance via integral term as proposed in (Borhaug et al., 2008).

8. Computational time

The PID controller needs to compute the error, integral and derivative of the error to compute the desired control input after multiplying with the gains. The control inputs can be computed within an order of

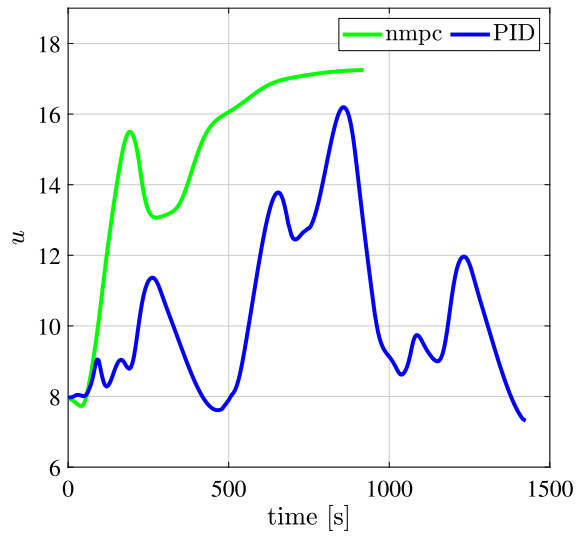

Fig. 28. Surge velocity.

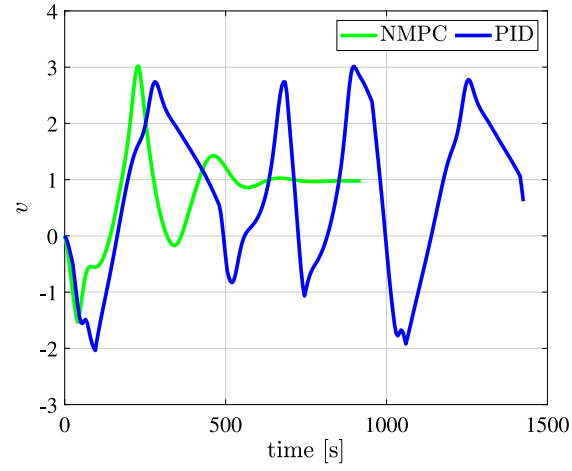

Fig. 29. Sway velocity.

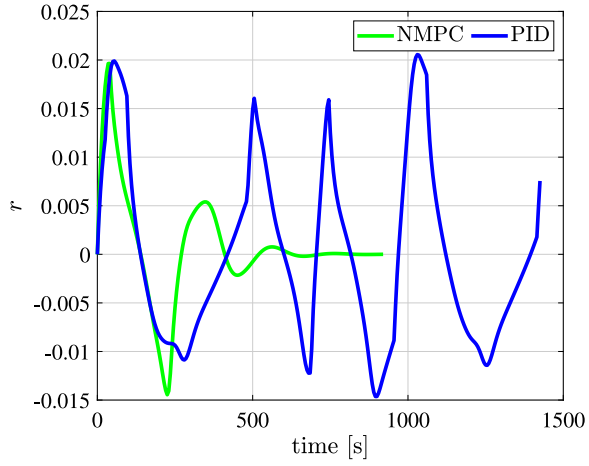

Fig. 30. Yaw rate.

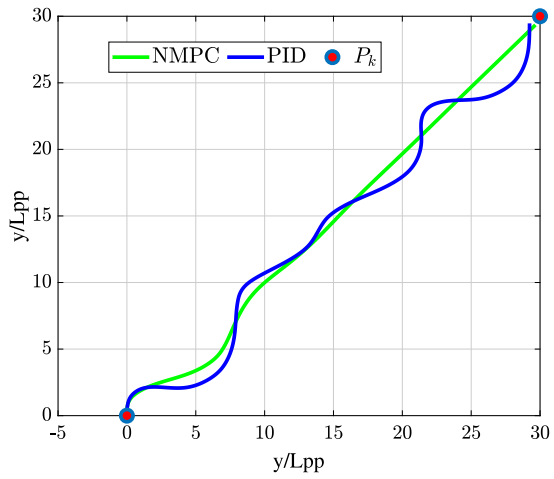

Fig. 31. Path following.

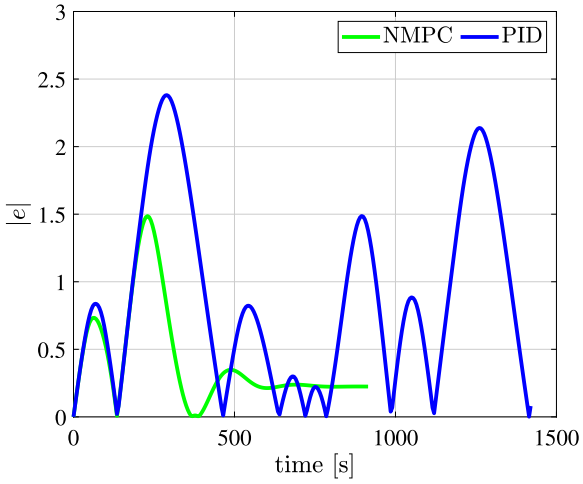

Fig. 32. Cross track error.

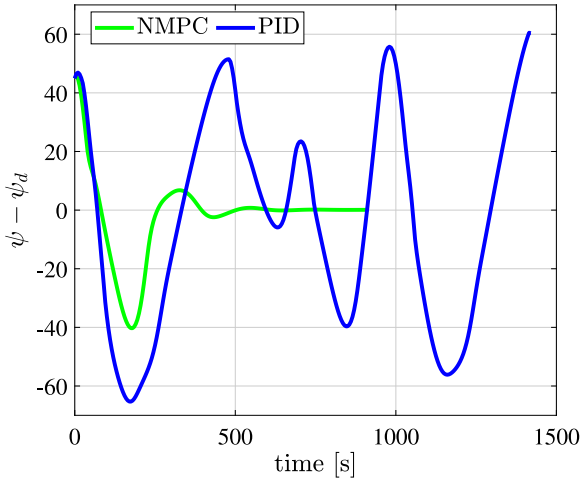

Fig. 33. Error in heading.

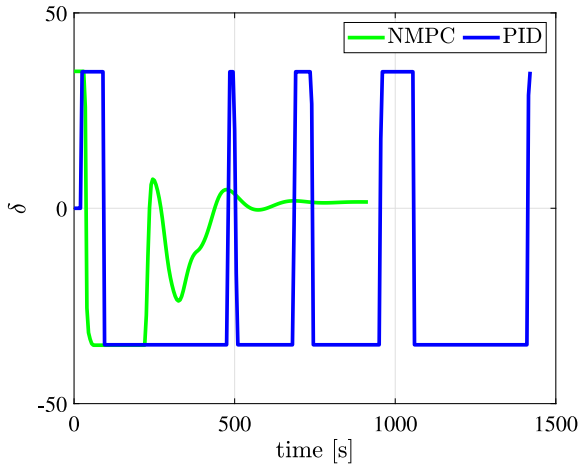

Fig. 34. Rudder deflection.

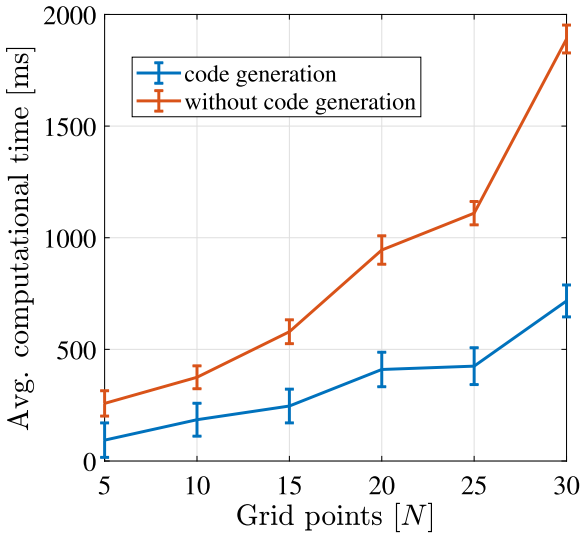

Fig. 35. Average computational time for optimization.

μs. However, for MPC, an expensive optimization problem is solved, which involves multiple iterations before converging to a solution. The average computational time taken in milliseconds to solve the optimization problem is given in Fig. 35 for different grid sizes. As shown in the plots, the computational time increases with grid size because a larger optimization problem needs to be solved. Even for grid size $N = 30$ (optimization problem with 240 variables), a runtime of 2 s is observed. This is possible due to efficient computations of the derivatives by automatic differentiation and the use of a sparse solver. To take further advantage, the functions are converted to C-programs and called from MATLAB using MEX files. The faster evaluation of the functions lowers the computational time significantly. With code generation, all grid sizes correspond to solve time of less than a second, which corresponds to the sampling time. Hence it is possible to compute solutions to the optimization problem in real-time before the next measurement update. The error bar indicates the standard deviation of the measurements and the worst-case time is also observed to be less than the sampling time of the system. The results are promising for experimental validations of the controller in future. All the simulations are carried out on a system with AMD ryzen 4600H and 8 GB of RAM.

9. Conclusions

A unified seakeeping and manoeuvring numerical model is integrated with a nonlinear MPC controller for predicting the manoeuvring of a KVLCC2 tanker in regular waves. The numerical simulations are conducted for path following problems based on waypoint navigation. The second order mean drift forces are computed based on strip theory and are calculated as a function of the wave frequency ω and wave encountering angle χ. The second order forces affect the surge, sway and yaw motions of the ship. A spline-based look-up table is constructed in order to use it in the numerical simulation.

First, Open-loop simulations are carried out in calm water and the results are compared with the available experimental data and validated. Similarly, open-loop numerical simulations for the trajectory of the ship in regular waves are conducted, and the drifting distances and drifting angles are compared with the experimental ones. The drifting distance decreases as the wavelength increases. The numerical simulation follows a similar trend except for the shortest wave. The largest drifting angle is observed for the longest wave for both the numerical and experimental results. For regular waves with $\lambda/L_{pp} = 1$, the error in the numerical prediction of the drifting distance and drifting angle is found approximately to be 10 %.

Next, the manoeuvring model is integrated with a nonlinear MPC controller for path following. A LOS algorithm computes the desired heading for nonlinear MPC controller and optimal rudder deflection is computed. Closed-loop simulations are carried out in calm water and regular waves for head and beam wave conditions. Nonlinear MPC is shown to track the desired trajectory. The nonlinear MPC controller is compared with a basic PID controller and advantages of the MPC controller are studied. The implementation of NMPC results in a lesser error in heading angle and rudder deflection compared to PID. Finally, the controller is tested in high seas with a wave steepness of 0.05 for heading control. NMPC is found to be effective in attaining the desired heading control and lower cross-track even in high sea states without additional tuning. A feasibility analysis of the controller is performed by studying the computational time taken to solve the optimization problem. By exploiting the sparsity of the optimization problem and using code generation, real-time solutions to the NMPC problem are achievable.

CRediT authorship contribution statement

R. Sandeepkumar: Conceptualization, Methodology, Software, Validation, Writing – original draft, Writing – review & editing. **Suresh Rajendran:** Conceptualization, Methodology, Validation, Writing – review & editing, Supervision. **Ranjith Mohan:** Conceptualization, Writing – review & editing, Supervision. **Antonio Pascoal:** Writing – review & editing.

Declaration of competing interest

The authors declare that they have no known competing financial interests or personal relationships that could have appeared to influence the work reported in this paper.

Acknowledgements

This project is funded by the Science and Engineering Research Board (SERB) under the project no: CRG/2018/004807 and SPARC Project No: SPARC/2018-2019/P935/SL for funding foreign faculty.

References

Andersson, J.A., Gillis, J., Horn, G., Rawlings, J.B., Diehl, M., 2019. CasADi: a software framework for nonlinear optimization and optimal control. Math. Program. Comput. 11 (1), 1–36.

Bailey, P., 1997. A unified mathematical model describing the maneuvering of a ship travelling in a seaway. Trans. RINA 140, 131–149.

Bertram, V., 2012. Practical Ship Hydrodynamics. Elsevier.

Borhaug, E., Pavlov, A., Pettersen, K.Y., 2008. Integral LOS control for path following of underactuated marine surface vessels in the presence of constant ocean currents. In: 2008 47th IEEE Conference on Decision and Control. IEEE, pp. 4984–4991.

Dagum, L., Menon, R., 1998. Openmp: an industry standard API for shared-memory programming. IEEE Comput. Sci. Eng. 5 (1), 46–55.

Fang, M.-C., Luo, J.-H., Lee, M.-L., 2005. A nonlinear mathematical model for ship turning circle. J. Ship Res. 49 (2), 69–79.

Fannemel, Å.V., 2008. Dynamic Positioning by Nonlinear Model Predictive Control (Master's thesis). Institutt for teknisk kybernetikk.

Fossen, T.I., 2005. A nonlinear unified state-space model for ship maneuvering and control in a seaway. Int. J. Bifurcation Chaos 15 (09), 2717–2746.

Griewank, A., Walther, A., 2008. Evaluating Derivatives: Principles and Techniques of Algorithmic Differentiation. SIAM.

Guerreiro, B.J., Silvestre, C., Cunha, R., Pascoal, A., 2014. Trajectory tracking nonlinear model predictive control for autonomous surface craft. IEEE Trans. Control Syst. Technol. 22 (6), 2160–2175.

Hasnan, M., Yasukawa, H., Hirata, N., Terada, D., Matsuda, A., 2019. Study of ship turning in irregular waves. J. Marine Sci. Technol. 1–20.

Kim, D.J., Yun, K., Park, J.-Y., Yeo, D.J., Kim, Y.G., 2019. Experimental investigation on turning characteristics of KVLCC2 tanker in regular waves. Ocean Eng. 175, 197–206.

Kouzoupis, D., Frison, G., Zanelli, A., Diehl, M., 2018. Recent advances in quadratic programming algorithms for nonlinear model predictive control. Vietnam J. Math. 46 (4), 863–882.

Lekkas, A.M., Fossen, T.I., 2013. Line-of-sight guidance for path following of marine vehicles. Adv. Marine Robot. 63–92.

Lewis, E., of Naval Architects, S., (U.S.), M.E., 1988. Principles of Naval Architecture: Motions in Waves and Controllability. In: Catalogued Knovel hcf, Society of Naval Architects and Marine Engineers, URL https://books.google.co.in/books?id=1mwZAQAAIAAJ.

Li, Z., 2009. Path Following with Roll Constraints for Marine Surface Vessels in Wave Fields (Ph.D. thesis). University of Michigan.

Li, Z., Sun, J., 2011. Disturbance compensating model predictive control with application to ship heading control. IEEE Trans. Control Syst. Technol. 20 (1), 257–265.

Liu, J., Allen, R., Yi, H., 2011. Ship motion stabilizing control using a combination of model predictive control and an adaptive input disturbance predictor. Proc. Inst. Mech. Eng. I: J. Syst. Control Eng. 225 (5), 591–602.

Molland, A., Turnock, S., 2002. Flow straightening effects on a ship rudder due to upstream propeller and hull. Int. Shipbuild. Prog. 49 (3), 195–214.

Moradi, M., Katebi, M., 2001. Predictive PID control for ship autopilot design. IFAC Proc. Vol. 34 (7), 375–380.

Moreira, L., Soares, C.G., 2011. Autonomous ship model to perform manoeuvring tests. J. Maritime Res. 8 (2), 29–46.

Nomoto, K., Taguchi, K., 1957. On steering qualities of ships (2). J. Zosen Kiokai 1957 (101), 57–66.

Oh, S.-R., Sun, J., 2010. Path following of underactuated marine surface vessels using line-of-sight based model predictive control. Ocean Eng. 37 (2–3), 289–295.

Oltmann, P., 1993. Roll-an often neglected element of manoeuvring. In: MARSIM '93, Intl Conf on Marine Simulation & Ship Manoeuvrability.

Ottosson, P., Bystrom, L., 1991. Simulation of the dynamics of a ship maneuvering in waves. Trans. Soc. Naval Archit. Marine Eng. 99, 281–298.

Perera, L., Moreira, L., Santos, F., Ferrari, V., Sutulo, S., Soares, C.G., 2012. A navigation and control platform for real-time manoeuvring of autonomous ship models. IFAC Proc. Vol. 45 (27), 465–470.

Peric, M., Bertram, V., 2011. Trends in industry applications of computational fluid dynamics for maritime flows. J. Ship Product. Design 27 (4).

Rawlings, J.B., Mayne, D.Q., Diehl, M., 2017. Model Predictive Control: Theory, Computation, and Design. vol. 2, Nob Hill Publishing Madison, WI.

Salvesen, N., 1974. Second-order steady-state forces and moments on surface ships in oblique regular waves. In: Int Symp. on the Dynamics of Marine Vehicles and Structures in Waves.

Seo, M.-G., Kim, Y., 2011. Numerical analysis on ship maneuvering coupled with ship motion in waves. Ocean Eng. 38 (17–18), 1934–1945.

Skejic, R., Faltinsen, O.M., 2008. A unified seakeeping and maneuvering analysis of ships in regular waves. J. Marine Sci. Technol. 13 (4), 371–394.

Skjetne, R., Smogeli, Ø.N., Fossen, T.I., 2004. A nonlinear ship manoeuvering model: Identification and adaptive control with experiments for a model ship. IFAC Proc. Vol..

Son, K., Nomoto, K., 1981. On the coupled motion of steering and rolling of a high speed container ship. J. Soc. Naval Archit. Japan 1981 (150), 232–244.

Sutulo, S., Guedes Soares, C., 2008. A generalized strip theory for curvilinear motion in waves. In: International Conference on Offshore Mechanics and Arctic Engineering. vol. 48234, pp. 359–368.

Sutulo, S., Soares, C.G., 2009. Computation of hydrodynamic loads on a ship manoeuvring in regular waves. In: Proceedings of the 10th International Conference on Stability of Ships and Ocean Vehicles.

Sutulo, S., Soares, C.G., 2019. On the application of empiric methods for prediction of ship manoeuvring properties and associated uncertainties. Ocean Eng. 186, 106111.

Tomera, M., 2017. Fuzzy self-tuning PID controller for a ship autopilot. In: Proceedings of the 12th International Conference on Marine Navigation and Safety of Sea Transportation.

Wächter, A., Biegler, L.T., 2006. On the implementation of an interior-point filter line-search algorithm for large-scale nonlinear programming. Math. Program. 106 (1), 25–57.

Xiang, X., Faltinsen, O.M., 2011. Maneuvering of two interacting ships in calm water. Marine Syst. Ocean Technol. 6 (2), 65–73.

Yasukawa, H., Nakayama, Y., 2009. 6-DOF motion simulations of a turning ship in regular waves. In: International Conference on Marine Simulation and Ship Manoeuvrability, Panama Panama city.

Yasukawa, H., Yoshimura, Y., 2015. Introduction of MMG standard method for ship maneuvering predictions. J. Marine Sci. Technol. 20 (1), 37–52.

Yen, T., Zhang, S., Weems, K., Lin, W., 2010. Development and validation of numerical simulations for ship maneuvering in calm water and in waves. In: Proceedings of the 28th Symposium on Naval Hydrodynamics, California USA, pp. 12–27.

Yoshimura, Y., 2001. Investigation into the yaw-checking ability in ship manoeuvability standard. Kijima, K.

Zheng, H., Negenborn, R.R., Lodewijks, G., 2014. Trajectory tracking of autonomous vessels using model predictive control. IFAC Proc. Vol. 47 (3), 8812–8818.